ISSN (Print) 1226-1750
ISSN (Online) 2233-6656
Journal of Magnetics 26(4), 429-436 (2021) https://doi.org/10.4283/JMAG.2021.26.4.429

Evaluation of Ultra-low-dose (ULD) Lung Computed Tomography (CT) Using Deep-learning: A Phantom Study

Daehong Kim[1], Kihong Son[2], Cheol-Ha Baek[3], Pil-Hyun Jeon[4]*, and Sooyeul Lee[2]

[1]Department of Radiological Science, Eulji University, Seongnam 13135, Republic of Korea
[2]Medical Information Research Section, Electronics and Telecommunications Research Institute, Daejeon 34129, Republic of Korea
[3]Department of Radiological Science, Kangwon National University, Samcheok 25949, Republic of Korea
[4]Department of Diagnostic Radiology, Yonsei University Wonju College of Medicine, Wonju Severance Christian Hospital, Wonju 26426, Republic of Korea

(Received 12 October 2021, Received in final form 17 December 2021, Accepted 18 December 2021)

As an electromagnetic wave, X-rays are used to acquire diagnostic CT images. The aim of this phantom study was to evaluate the image quality of ultra-low-dose (ULD) lung computed tomography (CT) achieved using a deep-learning based image reconstruction method. The chest phantom was scanned with a tube voltage of 100 kV for various CT dose index (CTDIvol) conditions: 0.4 mGy for ultra-low-dose (ULD), 0.6 mGy for low-dose (LD), 2.7 mGy for standard (SD), and 7.1 mGy for large size (LS). The signal-to-noise ratio (SNR) and noise values in reconstructions produced via filtered back projection (FBP), iterative reconstruction (IR), and deep convolutional neural network (DCNN) were computed for comparison. The quantitative results of both the SNR and noise indicate that the adoption of the DCNN makes the image reconstruction in the ULD setting more stable and robust, achieving a higher image quality when compared with the FBP algorithm in the SD condition. Compared with the conventional FBP and IR, the proposed deep learning-based image reconstruction approach can improve the ULD CT image quality while significantly reducing the patient dose.

Keywords : electromagnetic wave, Computed tomography (CT), low-dose, deep learning, image quality

1. Introduction

Computed tomography (CT) is widely used for the diagnosis of diseases, and has been increasingly utilized in the radiation oncology clinic because of the short examination time and resulting three-dimensional representation of the anatomical structure of the human body. However, an excessive reliance on CT examinations or the careless management of CT scanning dose protocols may carry avoidable health risks. Therefore, methods to reduce patient dose while maintaining CT image quality are being discussed by several researchers.

An obvious approach to this problem is the adoption of low-dose CT scanning protocols, for which methods such as automatic self-release control [1], tube current control [2], and tube voltage optimization [3] have been explored. In particular, research on standardizing or optimizing dose protocols for each part of the body is recognized as important [4].

In terms of hardware-based approaches to low-dose CT, there are efforts such as the development of a photon count-based detector [5]. The photon counting detector can acquire an image with reduced electronic noise, and studies on the removal of artifacts in clinical images using energy fractionation are being actively conducted [6].

Software-based efforts to develop a reconstruction method using sparse sampling for realizing low-dose CT images are also reported. There is a compressed sensing theory that perfect signal restoration is possible if the compressed matrix satisfies a certain condition, even when the number of measured data is remarkably small. The biggest advantage of sparse sampling is the effect of reducing patient dose by reducing the number of data samples [7].

With the increase in computation power enabled by hardware acceleration, iterative reconstruction methods are widely used in clinical practice to maintain image quality while significantly reducing noise in low-dose settings [8]. However, iterative reconstruction methods

*Corresponding author: Tel: +82-33-741-1499
Fax: +82-33-732-8281, e-mail: iromeo@yonsei.ac.kr

suffer from smoothing artifacts that negatively affect the resulting image quality [9]. Recently, a deep learning-based reconstruction method that can improve image quality while achieving more dose reduction than iterative reconstruction has been used. Deep learning-based reconstruction achieves higher image quality, lower dose, and faster reconstruction speeds than iterative reconstruction, and can produce more natural images [10].

Therefore, the purpose of this study is to evaluate the image quality achieved using deep learning reconstruction provided by the CT equipment at several doses based on CT dose index (CTDIvol) conditions used in clinical lung scans. The dose criteria used for lung imaging were CTDIvol 0.4 mGy for ultra-low-dose (ULD), CTDIvol 0.6 mGy for low-dose (LD), CTDIvol 2.7 mGy for standard dose (SD), and CTDIvol 7.1 mGy for a large-size patient (LS). Based on these dose protocols, the chest phantom was scanned, and the noise and signal-to-noise ratio (SNR) were evaluated after reconstructing the chest phantom image using filtered back projection (FBP), iterative reconstruction (IR), and deep convolutional neural network (DCNN).

2. Materials and Methods

2.1. Image reconstruction method

The image reconstruction methods used in this study are FBP, IR, and DCNN. Figure 1 shows the characteristics of each reconstruction method. FBP is a method of continuously summing the values of the projected images obtained in each direction by propagating intensities backwards in the image domain. In the back projection process, blurring inevitably occurs around the object being imaged, requiring the introduction of a filter to remove it. The iterative reconstruction method used here involves statistical iterative reconstruction algorithm. After comparing neighboring projections using a statistical model to find projections that are either overly noisy or photon-starving, which are replaced or modified so that the data achieves maximum consistency. The modified projection is assigned a lower weight to avoid potential bias, so that the modified projection contributes less to the reconstructed image than the unaltered projection. After conversion to the image domain by FBP, the image data is iteratively filtered using the statistical models of the noise structure. To this end, edge-preserving filter is applied to minimize the effect on the microstructure depiction and low-contrast detail [11]. The deep learning-based reconstruction method integrates an iterative reconstruction algorithm with a DCNN model that has been trained in the CT reconstruction task by pre-learning from a vast number of images. DCNN acquires data under optimized conditions and reconstructs high-quality CT images with model-based iterative reconstruction (MBIR). In addition, the DCNN trains image data corrupted by corresponding artifacts and simulated noise at low doses. Finally, the image is reconstructed using DCNN, a deep neural network, by simultaneously learning the reconstructed high-definition image by MBIR and the low-quality image without noise removal. This method has the advantage of reducing the image reconstruction time by about 1/3 compared to the model-based iterative reconstruction method while still achieving a high image quality in the resulting reconstructions [12]. The image reconstruction time of the CT used in this study was 15, 21, and 50 seconds, respectively, for FBP, IR, and DCNN

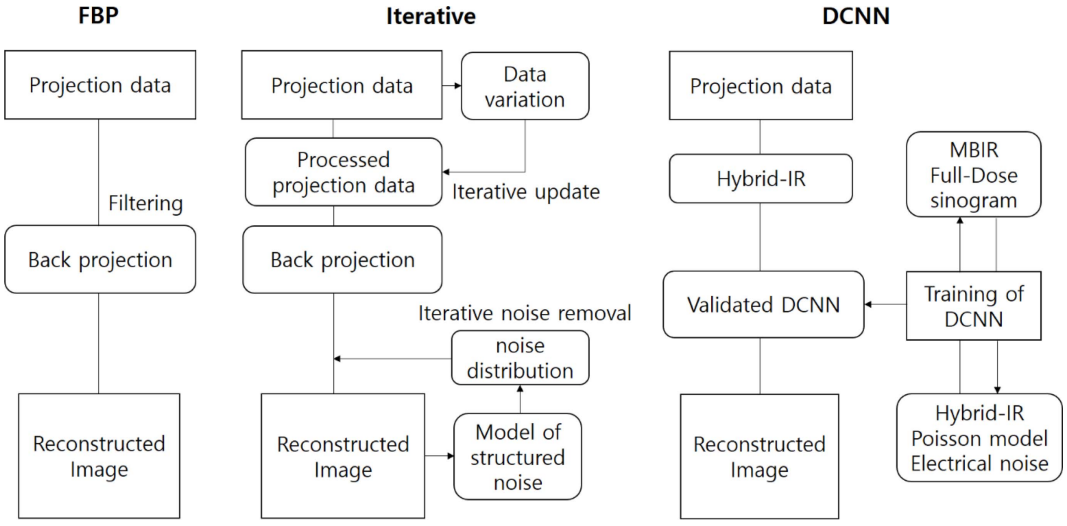

Fig. 1. Process diagrams for the filtered back projection (FBP), iterative reconstruction (IR), and deep convolutional neural network (DCNN) image reconstruction algorithms.

Table 1. Parameters of CT scans for this study.

Parameters	FBP	Iterative	Deep learning
Scan region	Upper, Middle, Lower	Upper, Middle, Lower	Upper, Middle, Lower
Tube potential (kV)	100	100	100
Slice thickness (mm)	1	1	1
Image matrix	512 × 512	512 × 512	512 × 512
CTDIvol (mGy)	0.4, 0.6, 2.7, 7.1	0.4, 0.6, 2.7, 7.1	0.4, 0.6, 2.7, 7.1

based on 1,000 image.

2.2. Image Acquisition Conditions

Table 1 shows the imaging conditions used in this experiment. CT acquisitions (Aquilion ONE GENESIS, Canon Medical Systems, Japan) of a human thorax phantom (Lungman, Kyoto Kagaku, Japan) were used to assess the image quality achieved through each of the reconstruction approaches. The Lungman phantom simulates the anatomical structure of the human thorax and includes soft tissues, spine, ribs, and blood vessels. Acquisitions of three phantom regions–the upper region including the apex of the lungs, the middle region containing the heart, and the lower region including the liver and diaphragm–were performed under the same tube voltage, the same slice thickness, and the same image matrix conditions. For all CT images, the tube voltage was set to 100 kV, the slice thickness was 1 mm, and the matrix of the CT images was set to 512 × 512. In order to capture the performance of each image reconstruction method under varying dose levels, the CT images were acquired using multiple scanning protocols. The CTDIvol of a lung CT scan for a standard patient is recommended to be less than 3.0 mGy, while a CTDIvol of up to 5.6 mGy for larger patients is recommended [13]. In this study, images were taken at 0.4, 0.6, 2.7, and 7.1 mGy based on the CTDIvol that is clinically applied to patient examinations at Wonju Severance Christian Hospital. In another study, CTDIvol in the range of 0.33 to 0.39 mGy was used for ultra-low dose CT [14, 15], but the lowest CTDIvol used in practice at Wonju Severance Christian Hospital is 0.4 mGy. This dose is the minimum dose that can guarantee sufficient image quality despite the ultra-low dose. In addition, 0.6 mGy is used for low-dose CT examinations, and the standard CTDIvol for high-resolution CT imaging is adopted as 2.7 mGy. A CTDIvol of 7.1 mGy is the highest dose, which was set assuming that the patient was thick, such as an overweight patient.

2.3. Image analysis method

We analyzed noise characteristics and the SNR for the quantification of image quality in the upper, middle, and lower phantom regions reconstructed through FBP, IR, and DCNN. Noise characteristics were obtained by calculating the standard deviation of pixels in various regions-of-interest (ROIs) selected in the upper, middle, and lower

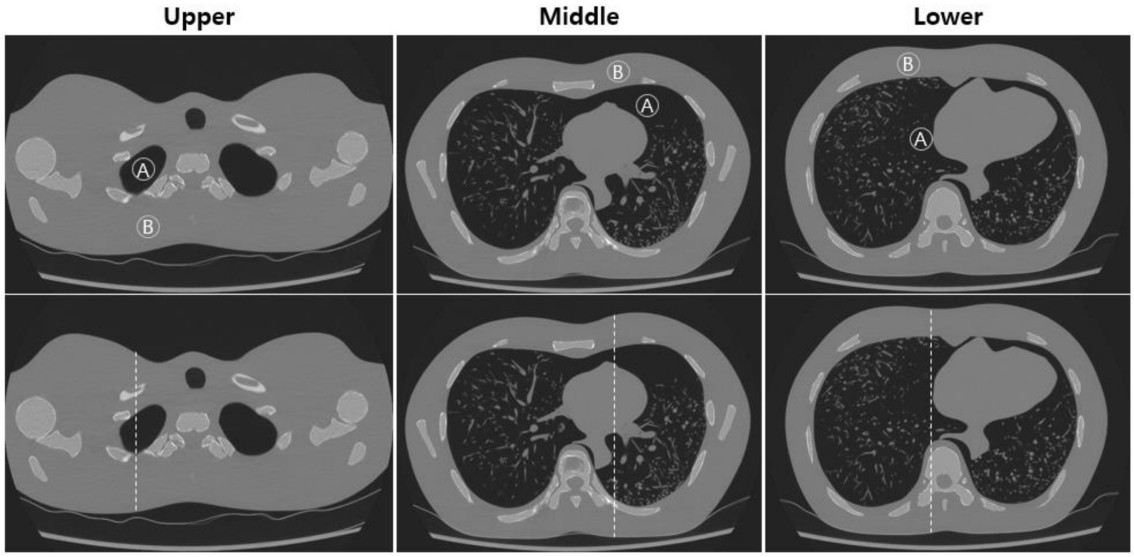

Fig. 2. ROI selected in the upper, middle, and lower regions of the phantom images for calculating SNR values (upper row). Dashed line selected in the upper, middle, and lower regions of the phantom images for image profiles (bottom row).

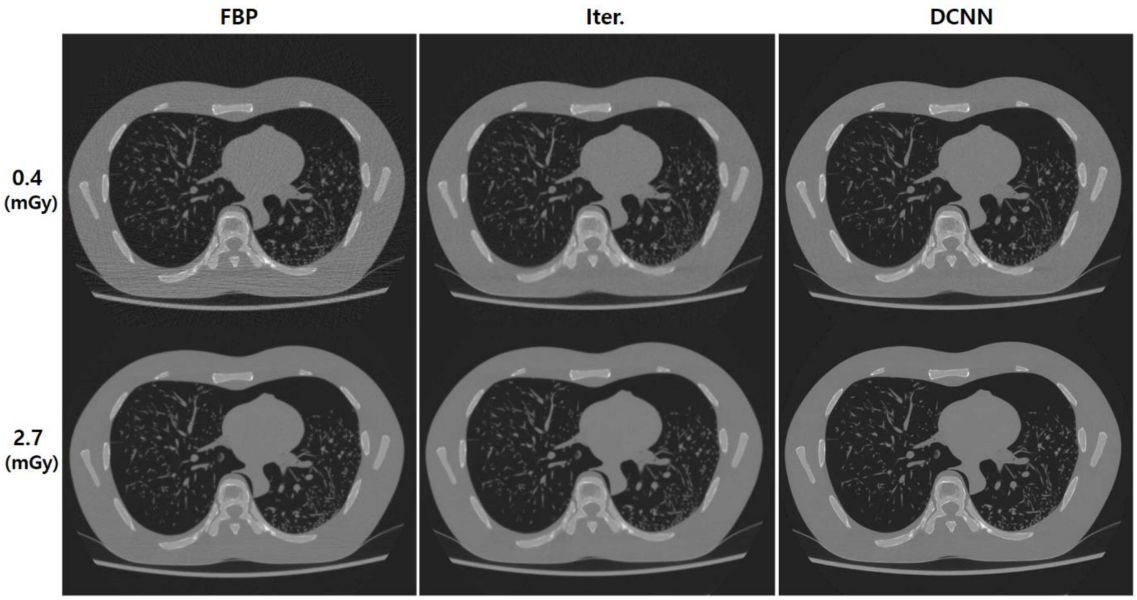

Fig. 3. Chest CT images reconstructed with filtered back projection (FBP), iterative reconstruction (IR), and deep convolutional neural network (DCNN) in the ultra-low-dose setting with a CTDIvol of 0.4 mGy (upper row) and the standard setting with a CTDIvol of 2.7 mGy (bottom row).

regions of the phantom. As seen in Fig. 2 (upper row), the SNR can be obtained by calculating the average value and standard deviation of the pixels in the ROI of the lung in the upper, middle, and lower images, and the average value of the pixels in the ROI of the tissue around the lung:

$$SNR = \frac{|M_{lung} - M_{tissue}|}{SD_{long}} \quad (1)$$

where M_{lung} is the average value of the pixels in the lung ROI, M_{tissue} is the average value of the pixels in the tissue ROI, and SD_{lung} is the standard deviation of the pixels in the lung ROI. In Fig. 2 (upper row), A is ROI of signal, and B is ROI of background for upper, middle, and lower images, respectively.

3. Results and Discussion

Figure 3 shows examples of FBP, IR, and DCNN images of the middle chest in the ultra-low dose setting with a CTDIvol of 0.4 mGy (upper row) and the standard dose condition with a CTDIvol of 2.7 mGy (bottom row). As can be observed in Fig. 3, the FBP reconstruction is greatly affected by noise when CTDIvol is 0.4 mGy but less so at the standard CTDIvol of 2.7 mGy. The trends of noise and SNR values in relation to changes in dose and choice of image reconstruction algorithm are shown in Figs. 4 and 5, respectively.

Figure 4 shows the noise values of FBP, IR, and DCNN reconstructions computed with respect to dose changes. Figure 4(a) shows the noise results of the upper region of the phantom, (b) the middle region, and (c) the lower region. In the images of all three phantom regions, the noise tends to decrease as the dose increases. At the same CTDIvol, the DCNN reconstruction is characterized by the lowest noise, followed by IR and FBP. At the standard CTDIvol dose of 2.7 mGy in Fig. 4(a), DCNN showed noise reduction of about 81.4 % compared to FBP, and noise reduction of about 39.4 % compared to IR. DCNN showed a noise value of 17.90 at the ultra-low dose CTDIvol of 0.4 mGy. At the standard CTDIvol of 2.7 mGy, the noise was reduced by about 67.0 % compared to the FBP, and when the maximum CTDIvol was 7.1 mGy, the noise was reduced by 49.7 % with the adoption of the DCNN over FBP.

Figure 4(b) shows the noise results according to the dose in the image of the middle lung. At the standard CTDIvol of 2.7 mGy, DCNN demonstrates a 51.9 % noise reduction compared to FBP. At the ultra-low-dose CTDIvol of 0.4 mGy, DCNN achieves a 4.8 % noise reduction compared to FBP in the standard setting with a CTDIvol of 2.7 mGy. However, one may observe that the ultra-low dose of 0.4 mGy DCNN increased the noise by about 38.7 % compared to the FBP at the maximum CTDIvol of 7.1 mGy.

Figure 4(c) shows the changes in noise with the dose in the image of the lower lung. At the standard CTDIvol of 2.7 mGy, DCNN showed a 41.8 % noise reduction com-

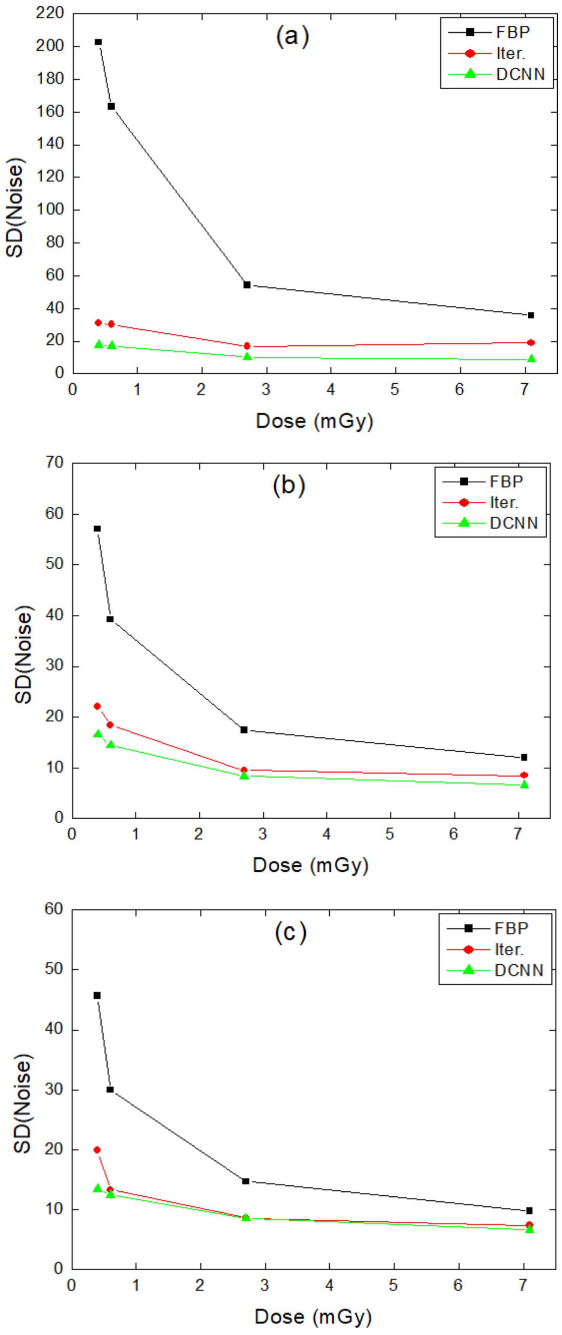

Fig. 4. (Color online) Computed noise values plotted against CTDIvol dose in reconstructions of the chest phantom in the (a) upper, (b) middle, and (c) lower regions.

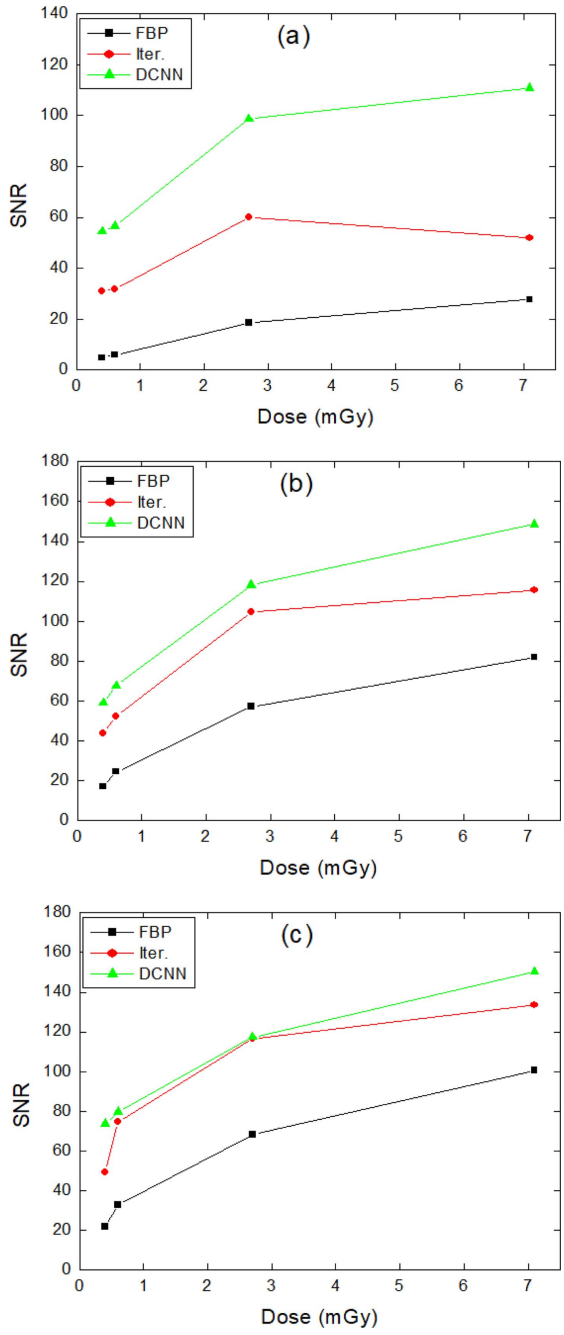

Fig. 5. (Color online) Computed signal-to-noise ratio (SNR) values plotted against CTDIvol dose in reconstructions of the chest phantom in the (a) upper, (b) middle, and (c) lower regions.

pared to FBP, and at the ultra-low-dose CTDIvol of 0.4 mGy, DCNN was able to achieve a 8.4 % noise reduction compared to FBP in the standard setting with a CTDIvol of 2.7 mGy. However, the ultra-low dose 0.4 mGy DCNN increased noise by about 37.5 % compared to the FBP at the maximum CTDIvol of 7.1 mGy. According to the noise results in Fig. 4, at the standard CTDIvol dose, DCNN shows a maximum noise reduction of 81.4 % and a minimum of 41.8 % compared to FBP. In addition, it was confirmed that the ultra-low dose CTDIvol 0.4 mGy showed better performance than the standard CTDIvol 2.7 mGy FBP imaging.

Figure 5 shows the changes in the SNR of the FBP, IR, and DCNN reconstructions with respect to dose changes. Figure 5(a) shows the SNR result of the upper region of

the phantom, (b) the middle part, and (c) the lower part. As the dose increases, the SNR tends to increase in most of the reconstruction results. At the same CTDIvol, the DCNN achieves the highest SNR, followed by IR and FBP.

Figure 5(a) shows the SNR result according to the dose change in the upper lung image. At the standard CTDIvol of 2.7 mGy, the SNR of DCNN was increased by about 431.8 % compared to that of FBP in the same dose setting. The result of the DNCC in the ultra-low-dose setting showed an increase in SNR of about 193.8 % compared to FBP in the standard setting with a CTDIvol of 2.7 mGy. Even compared with FBP at the maximum CTDIvol of 7.1 mGy, the SNR of the ultra-low-dose DCNN reconstruction was increased by about 96.7 %.

Figure 5(b) shows the SNR results according to the dose in the image of the middle lung. At the standard CTDIvol of 2.7 mGy, DCNN showed a 106.7 % increase in SNR compared to FBP, and at the ultra-low-dose CTDIvol of 0.4 mGy, DCNN achieved a 3.2 % increase in SNR compared to FBP at the standard CTDIvol of 2.7 mGy. However, the ultra-low-dose DCNN reconstruction reduced the SNR by about 28.1 % compared to the FBP at the maximum CTDIvol of 7.1 mGy.

Figure 5(c) shows the SNR results according to the dose in the image of the lower lung. At the standard CTDIvol of 2.7 mGy, DCNN showed an increase in SNR of about 71.8 % compared to FBP, and at the ultra-low-dose CTDIvol of 0.4 mGy, DCNN achieved an increase of about 8.0 % compared with FBP at the standard CTDIvol of 2.7 mGy. However, the ultra-low dose of 0.4 mGy DCNN showed a 26.6 % reduction in SNR compared to FBP at the maximum CTDIvol of 7.1 mGy. According to the SNR results in Fig. 5, at the standard CTDIvol, DCNN showed a maximum SNR increase of 431.8 % and a minimum of 71.8 % compared to FBP. In addition, the DCNN at the ultra-low dose CTDIvol of 0.4 mGy achieved better performance than FBP at the standard CTDIvol of 2.7 mGy.

This study quantitatively analyzed the effect on image quality of a deep learning-based reconstruction algorithm in ultra-low-dose chest CT to prove the possibility of future clinical applications. Depending on the location of the lungs, the image quality is different due to the artifacts caused by the bones around the lungs. Therefore, images of the upper, middle, and lower of the lungs were acquired because it was necessary to evaluate the image quality by level of the lungs. In clinical lung CT examination, the LD is set to approximately 1.2-1.5 mGy. In this study, the ULD was set to 0.4 mGy, which is about 1/3 lower than the LD. The reference dose for evaluating the image quality was set as the standard CTDIvol of 2.7 mGy for high-resolution CT imaging. The DCNN in the ultra-low-dose setting with a CTDIvol of 0.4 mGy showed superior performance in terms of noise reduction and SNR improvements compared to FBP in the standard setting with a CTDIvol of 2.7 mGy. This result means that when the deep learning reconstruction method is applied during CT examination, a dose reduction effect of at least about 85 % can be expected.

One of the advantages of deep learning image reconstruction is that it can reduce the image noise. As shown in Fig. 6, the FBP image in the ultra-low-dose setting with a CTDIvol of 0.4 mGy suffers from persistent reconstruction artifacts. This can make it difficult to distinguish noise from lesions such as pulmonary fibrosis. The deep learning algorithm can facilitate the discrimination of lung lesions by removing noise from the reconstructed lung image. Noise is also evaluated with image profile as seen in Fig. 2 (bottom row) dashed line. The profile

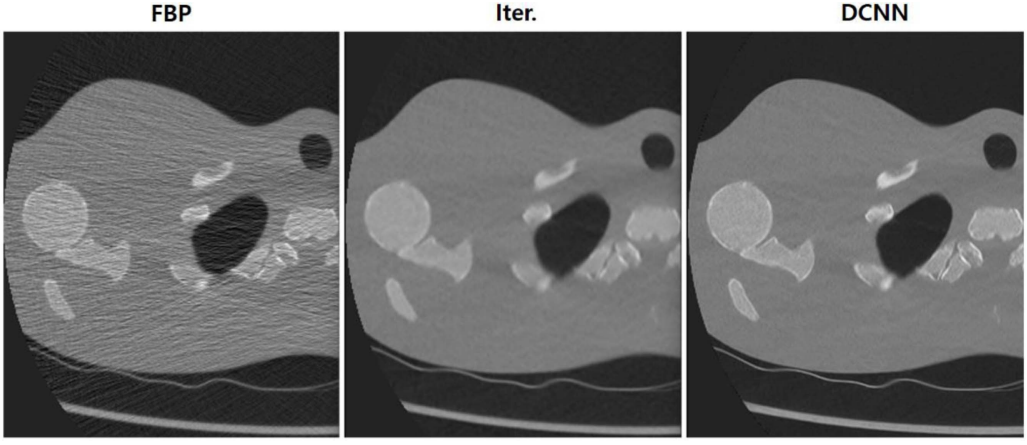

Fig. 6. Reconstructed images of the upper lung produced through filtered back projection (FBP), iterative reconstruction (IR), and deep convolutional neural network (DCNN) under a CTDIvol of 0.4 mGy for ultra-low-dose (ULD) CT.

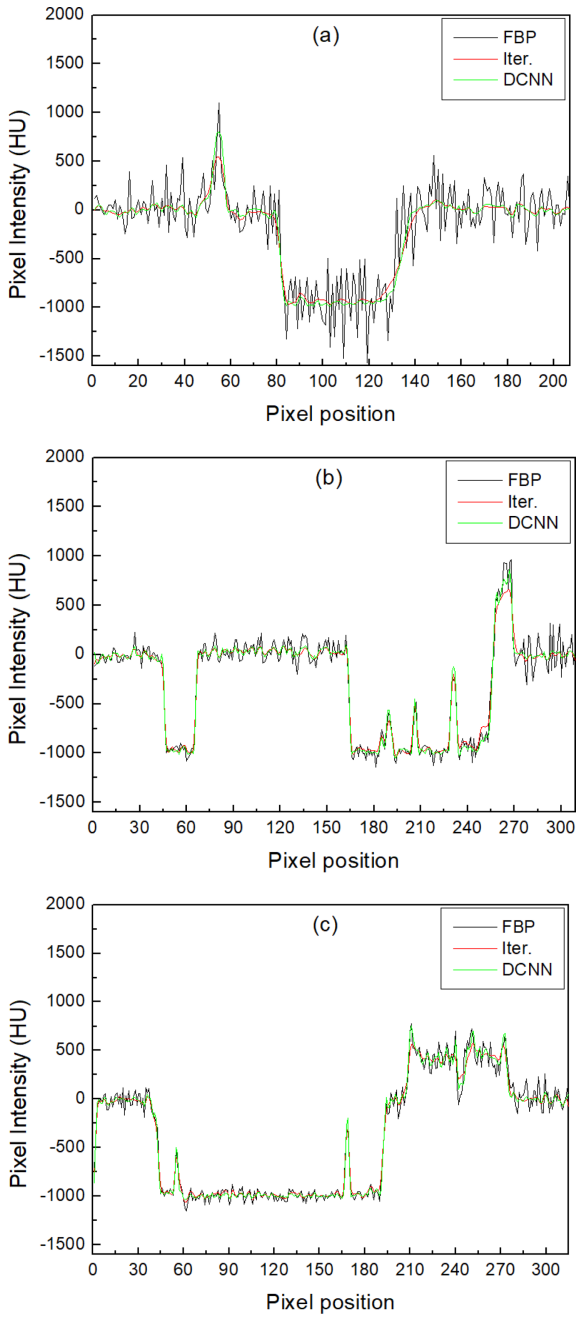

Fig. 7. (Color online) Image profiles are plotted in reconstructions of the chest phantom in the (a) upper, (b) middle, and (c) lower regions.

results are plotted in Fig. 7. Figures 7(a), (b), and (c) show the profile results measured in the upper, middle, and lower regions of the images acquired at an ULD setting with a CTDIvol of 0.4 mGy. According to the results, in all images, DCNN reduced noise effectively.

In general, a tube voltage of 120 kV is a common parameter choice in CT examinations. In this study, all images were acquired using a tube voltage of 100 kV. Since the radiation dose is roughly proportional to the square of the tube voltage, reducing the tube voltage can potentially reduce the radiation dose significantly. However, with the current technology, there is a limiting lower threshold for the tube voltage. For example, significant image quality deterioration has been reported due to beam hardening of the intravascular contrast medium during 80 kV imaging [16]. According to the results of the study by Fanous *et al.*, it is reported that reducing the tube voltage from 120 kV to 100 kV can reduce the radiation dose without significantly affecting the diagnostic image quality [17]. Therefore, in this study, a tube voltage of 100 kV was used, and it was confirmed that the deep learning-based image reconstruction method achieved great improvements in image quality.

A major limitation of our study is that the experimental conditions were limited by the geometry of the phantom to "average" patients. Imaging conditions for a patient with a thick body type were considered here with a CTDIvol up to 7.1 mGy, but the thickness of the phantom was unchanged, so it is difficult to accurately evaluate the image quality in the case of a larger patient. Therefore, further research is needed to improve the image quality of deep learning-based ultra-low-dose CT according to the thickness of the patient.

4. Conclusions

This study confirmed the superiority of the deep learning image reconstruction algorithm. The deep learning reconstruction has a significant noise reduction effect at low dose. Compared to the FBP and iterative reconstruction methods, the deep learning-based reconstruction method showed superior performance even in ultra-low-dose situations. In particular, the deep learning method provided superior image quality in terms of SNR than that of FBP in imaging of the upper lung region with severe bone streak artifact. Such a method is expected to offer a dramatic reduction of the patient's dose without significantly affecting the quality of the diagnostic image. In addition, the reduction of the image reconstruction time of deep learning due to the development of computing power can help in rapid examination, which is important in actual clinical imaging. According to the results of this study, the deep learning method is thought to contribute a lot to improving the image quality while reducing the radiation dose in clinical CT examinations.

Acknowledgment

This work was supported by ETRI (Electronics and

Telecommunications Research Institute)'s internal funds. [21YR2500, Development of Digital Biopsy Core Technology for high-precision Diagnosis and Therapy of Senile Disease]

References

[1] J. Greffier, F. Pereira, F. Macri, J.-P. Beregi, and A. Larbi, Phys. Med. **32**, 582 (2016).
[2] T. Kubo, Y. Ohno, M. Nishino, P.-J. Lin, S. Gautam, H.-U. Kauczor, H. Hatabu, and iLEAD study group, Eur. J Radiol. Open **3**, 86 (2016).
[3] T. Nakaura, M. Kidoh, S. Nakamura, Y. Doi, S. Shiraishi, K. Awai, K. Harada, and Y. Yamashita, Clin. Radiol. **69**, 804 (2014).
[4] S. Trattner, G. D. N. Pearson, C. Chin, D. D. Cody, R. Gupta, C. P. Hess, M. K. Kalra, J. M. Kofler Jr, M. S. Krishnam, and A. J. Einstein, J. Am. Coll. Radiol. **11**, 271 (2014).
[5] Z. Yu, S. Leng, S. Kappler, K. Hahn, Z. Li, A. F. Halaweish, A. Henning, and C. H. McCollough, J. Med. Imaging **3**, 043503 (2016).
[6] S. Leng, M. Bruesewitz, S. Tao, K. Rajendran, A. F. Halaweish, N. G. Campeau, J. G. Fletcher, and C. H. McCollough, RadioGraphics **39**, 729 (2019).
[7] Z. Hu and H. Zheng, BioMed. Eng. OnLine **13**, 70 (2014).
[8] C. Yan, J. Xu, C. Liang, Q. Wei, Y. Wu, W. Xiong, H. Zheng, and Y. Xu, Radiology **288**, 285 (2018).
[9] J. H. Kim, H. J. Yoon, E. Lee, I. Kim, Y. K. Cha, and S. H. Bak, Korean J. of Radiol. **22**, 131 (2021).
[10] C. M. McLeavy, M. H. Chunara, R. J. Gravell, A. Fauf, A. Cushnie, C. S. Talbot, and R. M. Hawkins, Clin. Radiol. **76**, 407 (2021).
[11] W. Stiller, Eur. J. Radiol. **109**, 147 (2018).
[12] M. Lenfant, O. Chevallier, P.-O. Comby, G. Secco, K. Haioun, F. Ricolfi, B. Lemogne, and R. Loffroy, Diagnostics **10**, 558 (2020).
[13] Lung cancer screening CT protocols Version 5.1, AAPM, (2019).
[14] K. Ye, M. Chen, J. Li, Q. Zhu, Y. Lu, and H. Yuan, Clin. Radiol. **76**, 156.e1 (2021).
[15] H. J. Wisselink, G. J. Pelgrim, M. Rook, K. Imkamp, P. M. A. van Ooijen, M. van den Berge, G. H. de Bock, and R. Vliegenthart, Eur. J. Radiol. **138**, 109646 (2021).
[16] Z. Szucs-Farkas, L. Kurmann, T. Strautz, M. A. Patak, P. Vock, and S. T. Schindera, Invest. Radiol. **43**, 871 (2008).
[17] R. Fanous, H. Kashani, L. Jimenez, G. Murphy, and N. S. Paul, Am. J. Roentgenol. **199**, 990 (2012).